Insight into Ribonuclease A Domain Swapping by Molecular Dynamics Unfolding Simulations†

Luciana Esposito*,‡ and Valerie Daggett*,§

Istituto di Biostrutture e Bioimmagini, CNR, Via Mezzocannone 16, I-80134 Napoli, Italy, and Department of Medicinal Chemistry, University of Washington, Seattle, Washington 98195-7610

Received June 7, 2004; Revised Manuscript Received September 29, 2004

ABSTRACT: Bovine pancreatic ribonuclease (RNase A) deserves a special place among the numerous proteins that form oligomers by three-dimensional domain swapping. In fact, under destabilizing conditions and at high protein concentrations, it can swap two different domains, the N-terminal α-helix or the C-terminal β-strand, leading to dimers with different quaternary structures. With the change in the unfolding conditions, the relative abundance of the two dimers varies, and the prevalence of one dimer over the other is inverted. To investigate the dynamic behavior of the termini, four independent 10 ns high-temperature molecular dynamics simulations of RNase A were carried out at two different pH values in an attempt to reproduce the experimental conditions of neutral and very low pH that favor the formation of the N- and C-terminal domain-swapped dimers, respectively. In agreement with experimental data, under mild unfolding conditions, a partial or complete opening of the N-terminal arm is observed, whereas the dislocation of the C-terminus away from the core of the structure occurs only during the low-pH simulations. Furthermore, the picture emerging from this study indicates that the same protein can have different pathways for domain swapping. Indeed, in RNase A the C-terminal swapping requires a substantial unfolding of the monomers, whereas the N-terminal swapping can occur through only partial unfolding.

The functional state of many proteins is an oligomeric assembly that has evolved to provide new properties with respect to the monomeric state. Domain swapping (DS) is a recently recognized mechanism for oligomerization, involving the mutual exchange of an identical domain (either an entire tertiary domain or a short segment) between polypeptide chains in the oligomer (*1*, *2*). This association mode results in the formation of an intersubunit interface (closed interface) that is identical to the intrasubunit interface in the monomer and an additional interface (open interface) that is unique to the domain-swapped form. Since Eisenberg and colleagues first described the domain-swapped form of the diphtheria toxin (*3*), more than 40 domain-swapped protein structures have been reported (*4*, *5*). The growing number and the large diversity of proteins that adopt a domain-swapped form as a native or a non-native structure has stimulated many questions with respect to the role, if any, of domain swapping (*4*−*6*). It has been proposed as a possible step in the evolutionary pathway from monomer to oligomer (*1*−*3*, *7*), as a mechanism for protein misfolding and aggregation, eventually leading to amyloid fibril formation (*8*−*12*), and also as a means of endowing proteins with regulatory or other biological functions (*13*, *14*).

The first report of dimer formation by intertwining of domains dates back to 1962 when Crestfield et al. observed that RNase A[1] (Figure 1A) forms dimers and higher-order aggregates after lyophilization in a 40−50% acetic acid solution (*15*). On the basis of an elegant biochemical experiment, they proposed that the dimer was formed by exchanging the N-terminal α-helix (Figure 1B). Later studies showed that, under those conditions, two types of dimers are formed (a major and a minor component) that exhibit different biochemical and biophysical properties as well as different quaternary structures (*16*, *17*). Both dimers are metastable and spontaneously and irreversibly dissociate into monomers. The crystal structures showed that the major dimer forms by exchanging the C-terminal β-strand (residues 116−124) (C-dimer) (Figure 1C) (*10*), whereas the minor component is a dimer formed by the intertwining of the N-terminal α-helix (residues 1−13) (*9*), just as hypothesized by Crestfield et al. (*15*) (N-dimer) (Figure 1B).

Given its ability to swap two different regions of the molecule, RNase A represents a peculiar and interesting example of domain swapping. The combination of the two modes of swapping in the same molecule can indeed lead to a variety of oligomers (*18*, *19*), among which there are also cyclic structures such as the one of a trimer recently determined by X-ray diffraction (*20*). The two dimeric forms

† This work was supported by the Human Frontier Science Program (Grant ST00135/2002 to L.E.), the CNR Short-term mobility program (to L.E.), and the National Institutes of Health (Grant GM50789 to V.D.).

* To whom correspondence should be addressed. E-mail: daggett@u.washington.edu or lucianaesposito@chemistry.unina.it.

‡ CNR.

§ University of Washington.

[1] Abbreviations: RNase A, bovine pancreatic ribonuclease; N-dimer, N-terminal domain-swapped dimer; C-dimer, C-terminal domain-swapped dimer; MD, molecular dynamics; rmsd, root-mean-square deviation; rmsf, root-mean-square fluctuation; CD, circular dichroism; FT-IR, Fourier transform infrared spectroscopy; SAXS, small-angle X-ray scattering.

10.1021/bi0488350 CCC: $30.25
Published on Web 02/12/2005

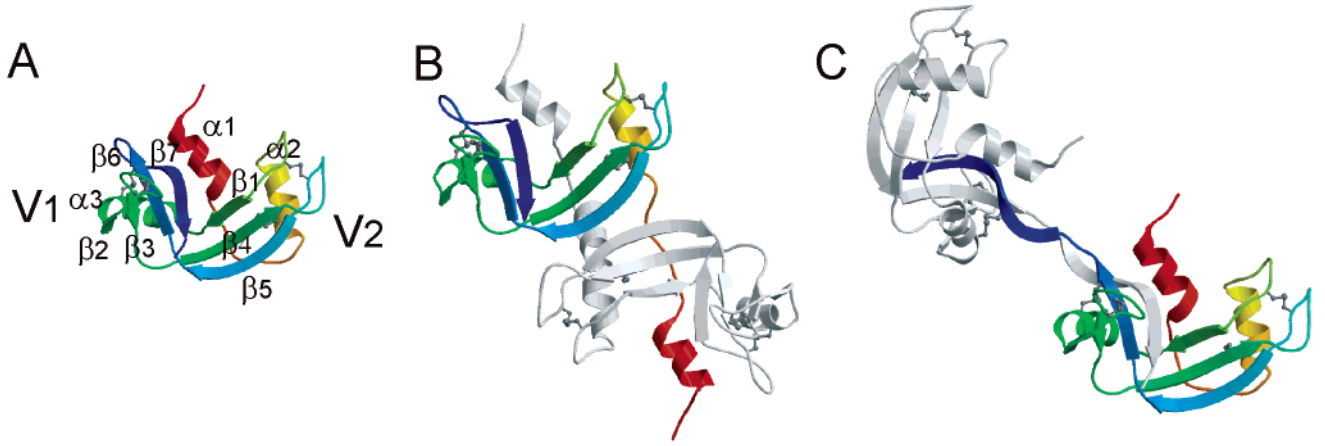

FIGURE 1: Ribbon schematic representations of (A) RNase A (PDB entry 1KF5), (B) the N-dimer (PDB entry 1AW2), and (C) the C-dimer (PDB entry 1F0V). Disulfide bonds, secondary structure elements, and the two arms of the V-shaped β-sheet motif (see Materials and Methods) are labeled on monomeric RNase A. The secondary structure elements defined in the PDB entries are used. The monomeric structures are colored from red at the N-terminus to blue at the C-terminus. In the dimers, one of the two chains is depicted in white. This figure was drawn with Molscript (*55*) and Raster3D (*56*).

of RNase A have received recent attention not only as a model for studying protein aggregation but also for their antitumor activity (*21*). A deeper understanding of the properties of these dimers has been gained from both molecular dynamics (MD) studies of the dimeric structures (*22*; L. Vitagliano, personal communication) and a more complete biochemical characterization of the experimental conditions that promote dimer formation (*23*). The latter studies have revealed a rather complex picture for RNase A oligomerization. As described above, the very low pH of acetic acid solutions (pH 1.0−1.5) together with the lyophilization process yields ~20% dimeric aggregates with the C-dimer prevailing over the N-dimer in a 4:1 ratio. Lyophilization of RNase A in water, however, gave no oligomeric products. Recent studies have shown that appreciable amounts of dimers can be formed even without the lyophilization step, but they required high protein concentrations (~200 mg/mL) and incubations at a high temperature (60 °C) (*23*). The authors illustrated that in some media (40% TFE or ethanol) the total amount of dimers is comparable to that obtained from the lyophilization procedure with a net prevalence of the C-dimer over the N-dimer (ratio of 2:1). However, lower amounts result in milder media (borate buffer at pH 8.5 or 10, bidistilled water, etc.) with an inversion of the relative proportions of the dimers. The authors suggested that harsh unfolding conditions favor the C-terminal swapping, whereas milder denaturing conditions favor the swapping of the N-terminal helix.

Here we describe MD simulations of the temperature-induced unfolding of monomeric RNase A in an effort to obtain clues about the dynamic behavior of the terminal segments of the protein. MD denaturing simulations at high temperatures have become a well-established tool for making predictions about the behavior of proteins under unfolding conditions (*24*). Previous MD unfolding simulations have been reported for a monomeric protein, p13suc1, which forms a domain-swapped dimer (*25*). The p13suc1 study suggested that the protein must undergo extensive unfolding for the swapping to occur.

Here we investigate RNase A, another small monomeric protein (124 residues and four disulfide bridges) whose structure has been extensively studied by X-ray crystallography, even at very high resolution (*26*, *27*). MD unfolding simulations were performed on the oxidized protein at 498 K at neutral pH and at very low pH to mimic the experimental conditions that favor the formation of either the N- or C-terminal domain-swapped dimer.

MATERIALS AND METHODS

The System. The RNase A structure consists of two antiparallel β-sheets that form a characteristic V-shaped motif [the two arms of the V are denoted as V1 and V2; V1, β1 (residues 43−47), β4 (residues 79−86), and β5 (residues 97−104); V2, β2 (residues 61−63), β3 (residues 72−74), β6 (residues 106−111), and β7 (residues 116−123)] and three helices [α1 (residues 3−13), α2 (residues 24−33), and α3 (residues 50−60)] packed against the central β-sheets. The C-terminal segment (residues 116−124) contains a β-strand and is connected to the body of the molecule by a type VI β-turn (residues 112−115) which acts as a hinge. The N-terminal segment (residues 1−14) contains an α-helix and is connected to α2 by a hinge loop (residues 15−22), which shows different conformations in the N-dimer subunits, adopting an α-helical structure in one of the two. The protein contains four disulfide bridges (from residue 58 to 110, residue 26 to 84, residue 40 to 95, and residue 65 to 72). The part of the protein structure not made up of the terminal segments is termed the "body" of the molecule throughout the paper.

MD Simulations. MD simulations in the presence of explicit water molecules were performed using ENCAD (*28*). The potential energy functions and MD protocols have been described (*29*, *30*). The phosphate-free X-ray structure of RNase A determined at pH 7.1 and 1.15 Å resolution was used as the starting model (PDB entry 1KF5) (*26*). Residues with alternative conformations in the crystal structure were included in the model using the highest-occupancy conformer. The crystal structure contains neutral histidine residues. In the low-pH simulation, the ionization state of the charged residue was set to mimic the pH of the 40−50% acetic acid solutions (pH 1.0−1.5) used in lyophilization experiments. Namely, all His, Lys, and Arg residues of the crystal structure were positively charged, and the acidic groups and the terminal carboxylate group were protonated.

Residual strain in the structure was relieved using 1000 steps of conjugate gradient minimization in vacuo. The protein was then solvated using a rectangular box extending at least 8, 10, or 12 Å in all directions (Wbox). Periodic boundary conditions were employed to reduce edge effects. The number of water molecules ranged from 3813 to 6276.

A temperature of 498 K was used for the unfolding simulations, and the water density was set to the corresponding experimental value of 0.829 mg/mL (*31*). Before the system was heated to 498 K, a preparatory stage was carried out which included the following steps in order: energy minimization steps (E_1w) of the solvent water, molecular dynamics steps of the water (MDw), and finally energy minimization steps of the solvent (E_2w), the protein (E_2p), and the protein−solvent system (Ep + w). Four high-temperature classical MD simulations were performed at neutral (N498_MD1−4) and low (L498_MD1−4) pH. A slightly different preparatory protocol was used for the four simulations to yield independent trajectories (N498_MD1, Wbox = 10 Å, E_1w = MDw = E_2w = Ep = Ep + w = 1000; N498_MD2, Wbox = 8 Å, E_1w = E_2w = Ep = Ep + w = 1000, MDw = 11 000; N498_MD3, Wbox = 12 Å, E_1w = MDw = E_2w = Ep = Ep + w = 1000; N498_MD4, Wbox = 12 Å, E_1w = E_2w = 1000, MDw = 9000, Ep = Ep + w = 500; L498_MD1, Wbox = 12 Å, E_1w = E_2w = 1000, Ep = Ep + w = 500, MDw = 6000; L498_MD2, Wbox = 8 Å, E_1w = E_2w = 1000, Ep = Ep + w = 1000, MDw = 5000; L498_MD3, Wbox = 8 Å, E_1w = E_2w = Ep = Ep + w = 1000, MDw = 10 000; L498_MD4, Wbox = 12 Å, E_1w = E_2w = Ep = Ep + w = 1000, MDw = 10 000). In one of the four low-pH simulations (L498_MD3), we tested the effect of adding counterions (chloride ions) to balance the +19 net charge of the protein molecule. The counterions were added by replacing water molecules with the highest electrostatic potentials. No significant variations were found.

Each simulation was carried out for 10 ns using a 2 fs integration time step. An 8 Å force-shifted nonbonding cutoff distance was used, and the nonbonded list was updated every five cycles. Control simulations at 298 K were performed at low and neutral pH (N298_MD and L298_MD, respectively). In this case, a 10 Å nonbonding cutoff distance was used, since the 8 Å value yielded unstable trajectories (using an 8 Å cutoff, after 10 ns the C_α rmsd from the starting structure was as high as ∼3.5 and ∼6 Å for the neutral and low-pH simulations, respectively). The preparatory protocols for both the room-temperature simulations were as follows: Wbox = 10 Å, E_1w = E_2w = Ep = Ep + w = 1000, MDw = 5000.

Our past studies and a recent analysis (*32*) have demonstrated that nonbonded spherical cutoff radii of 8 and 10 Å yield similar results with our force field with few exceptions. To accelerate the calculations, we used an 8 Å cutoff for the high-temperature simulations. We have found comparable results using 8 and 10 Å cutoffs at high temperatures given the reduced density of the system, which decreases the number of short electrostatic interactions.

RESULTS

Control Simulations at 298 K. Simulations (10 ns) were carried out at neutral (N298) and low pH (L298) at 298 K.

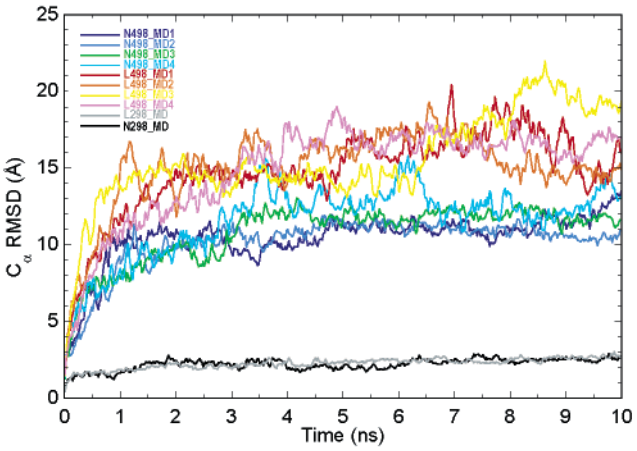

FIGURE 2: C_α rmsd from the starting structure as a function of simulation time averaged over 20 ps intervals. The 498 K neutral and low-pH simulations are depicted with blue or green and red or yellow colors, respectively.

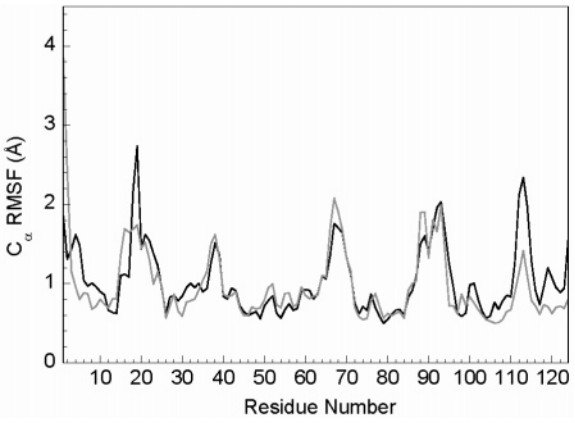

FIGURE 3: C_α rms fluctuation from the average position calculated for the 4−10 ns interval of the neutral (black) and low-pH (gray) native (298 K) simulation.

Both trajectories were found to be stable as reflected in the plateau reached by the C_α rmsd of the MD structures from the starting structure (Figure 2). The C_α rmsd, calculated in the equilibrated region of the trajectory (1.5−10 ns), is the same for the two 298 K simulations (2.3 ± 0.3 Å for N298 and 2.3 ± 0.2 Å for L298). The rms fluctuations for C_α atoms, calculated over the 4−10 ns time period, exhibit low values for most of the secondary structural elements (Figure 3).

Analysis of the main interactions that anchor the terminal segments to the rest of the molecule reveals that both segments are well fixed within the structure at the two different pHs. Indeed, in the native structure, the N-terminus is anchored by strong hydrogen bonds involving residues 12−14, at the end of helix α1, and residues 45−47, which belong to small beta strand β2 (i.e., NH47−O12, $N_{\delta1}$H12−O45, and NH14−O47). These three H-bonds are well preserved during the MD trajectories. Similarly, the C-terminus β7 strand is paired with the β6 strand by H-bonds which are very stable during the simulations.

An overall analysis of the main motions of the protein indicates that there is an "opening" of the two arms of the V-shaped β-sheet motif (Figure 1A). The distance between the nitrogen atoms of Thr45 and Phe120 was used previously to measure the magnitude of this breathing motion (*33*). In

our N298 simulation, this distance fluctuates around a mean value of 9.0 ± 0.8 Å. Interestingly, the opening is more pronounced at low pH, L298 (10.4 ± 0.7 Å).

High-Temperature MD Simulations at Neutral and Low pH: Global Unfolding Behavior. Four independent MD unfolding simulations were carried out at 498 K for 10 ns at both neutral (N498_MD1−4) and low pH (L498_MD1−4). At each pH, RNase A reaches a similar degree of unfolding, as is evident from some global parameters plotted as a function of time (Figure 2). At neutral pH, the C_α rmsd from the starting structure increases rapidly, reaching 8−9 Å around 1 ns. After this initial abrupt change, the C_α rmsd slowly increases over the following 4 ns and then stabilizes at a final value of ∼12 Å. A similar trend for other global properties, such as the number of native contacts and the surface accessibility area, is observed; i.e., the earliest hundreds of picoseconds of the unfolding process account for the largest change in the structural properties. For instance, the percentage of native contacts, averaged over the four simulations, drops to 54% after 600 ps, to 48% at 1 ns, and to about 42% at the end of the simulation.

At low pH, the unfolding is more rapid and leads to higher C_α rmsd values (Figure 2). The C_α rmsd from the starting structure is ∼13 Å at 1 ns and increases to ∼17 Å at the end of the simulation. The percentage of native contacts is 43% after 600 ps and 41% at 1 ns and stabilizes to a minimum value of 36%. Little change is observed at both pHs in the average values of the global properties after ∼4 ns, which we take as an indication that an unfolded state has been reached.

A common feature of the neutral and low-pH unfolding simulations is the rapid loss of most of the β-structure in the first nanosecond. Indeed, using an average over this period, the neutral and low-pH simulation structures contain 17 and 12% β-structure, respectively, with the central β-strands of both V1 and V2 β-sheets (β4 and β6, respectively) as the most stable strands. On the other hand, the stability of the three helices is remarkable, and residual helical structure is present in the denatured state after 10 ns. The average order of stability in the simulations is as follows: $\alpha2 > \alpha1 > \alpha3$.

High-Temperature MD Simulations at Neutral and Low pH: Dynamic Behavior of the Terminal Segments. Neutral pH. The analysis of MD trajectories here focuses on the behavior of the N- and C-terminal segments that swap to form the C- and N-dimers, respectively. There is no significant displacement of the C-terminus (residues 116−124) in any of the neutral pH simulations; a partial or complete opening of the N-terminus (residues 1−13) from the body of the molecule is found in N498_MD1 and N498_MD4 simulations. Therefore, a more detailed analysis of the latter events will be presented.

N498_MD1. The beginning of the N498_MD1 simulation is characterized by an expansion of the molecule and a displacement of the chain terminal segments. Helix α1 moves away from the rest of the molecule, and the β7 segment moves away from its adjacent β6 strand. There is also a separation of the α1 and the C-terminal β-hairpin (Figure 1A), which leads to loosening of the main hydrophobic core. A quantitative measure of the exposure of α1 to solvent has been derived by following the solvent accessible surface area (SASA) of Phe8, which is located at the center of the helix

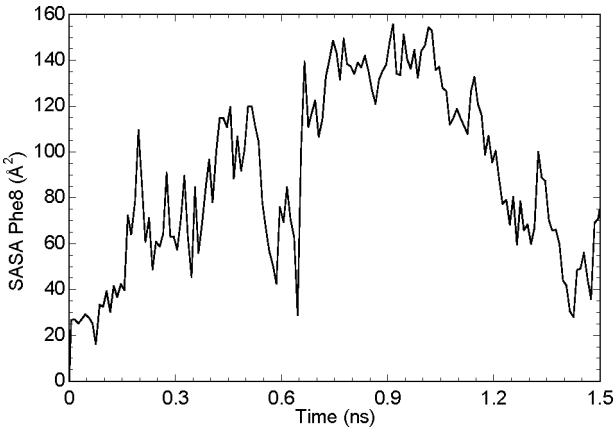

FIGURE 4: Solvent accessible surface area (SASA) for the Phe8 side chain calculated in the 0−1.5 ns interval by averaging over structures each 20 ps.

and tightly packed into the more extensive hydrophobic core. After an initial increase, the first relevant peak in the SASA curve is observed at ∼200 ps when the helix loses most of its native contacts with the two lobes of the V-shaped motif (Figure 4). By this time, the two stable H-bonds (12O−47NH and $12N_{\delta1}H-45O$) anchoring α1 to residues 45−47 are disrupted. The helix moves toward the V2 lobe of the molecule and fluctuates, but remains close to the α2 helix. Meanwhile, the C-terminal segment displays non-native charged interactions between Asp121 and Lys66 and between the terminal carboxylate group of Val124 and both Lys104 and Arg85. The latter residue retains its native ionic pair interaction with Asp83, thus forming a cluster of four charges, which restricts the mobility of the C-terminal segment.

From 200 to 1200 ps, the N-terminus experiences movements toward and away from the rest of the molecule, leading to alternating minimum and maximum values in Phe8 SASA (Figure 4). For instance, after an increase in the Phe8 SASA (∼400−500 ps), α1 is partially repacked to the V1 lobe of the molecule with Phe8 establishing hydrophobic interactions with residues Val47 and Leu51 and with Val116 and Pro114 of the C-terminal region. Again, the minimum of Phe8 SASA at 600 ps is followed by a substantial increase (∼660 ps) corresponding to the loss of the contacts between α1 and the C-terminus, and to a movement of the N-terminus toward α2 and the "back" of the molecule (i.e., the side of the molecule opposite the side of the active site cleft) (Figure 5A). Helix 1 also unwinds at its N-terminus and in its fluctuation displays interaction with the hinge region (residues 14−22) and with residues 41−47. At ∼880 ps, when these interactions are weakened, the N-terminus separates from the body of the molecule and only interacts with the solvent (Figure 5A).

This opening lasts ∼140 ps until the N-terminus collapses onto the molecule. In fact, due to a large fluctuation of the completely unwinded N-terminal region of the helix, Lys1 establishes an electrostatic interaction with Asp53. This initial link drives the formation of a new contact interface formed by evolving hydrophobic patches which involve the nonpolar side chains of Ala4, Ala5, Phe8, Leu54, and Leu51.

To better visualize the N-terminal opening, heavy atom contact maps are calculated for the time interval of 880−1020 ps and for the two 140 ps time periods immediately

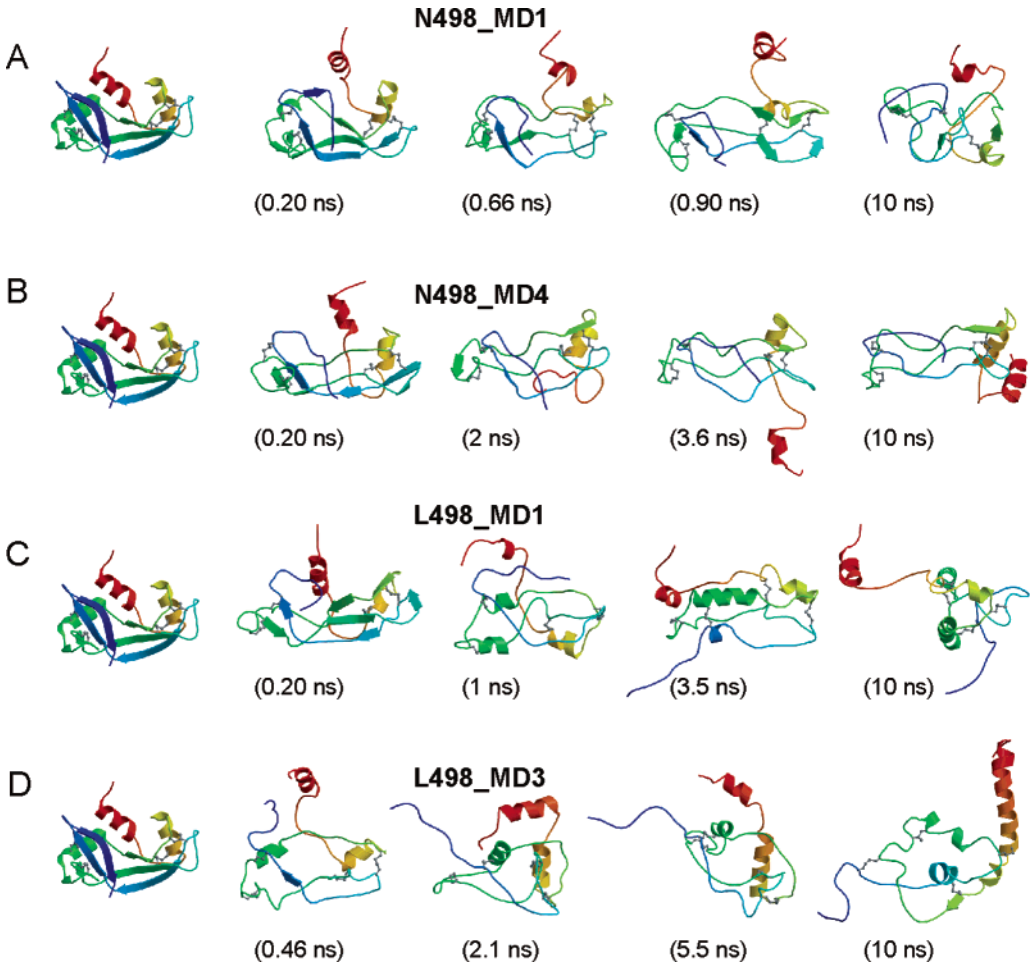

FIGURE 5: Snapshots of structures from unfolding simulations at neutral (A and B) and low pH (C and D): (A) N498_MD1 simulation, (B) N498_MD4 simulation, (C) L498_MD1 simulation, and (D) L498_MD3 simulation. The secondary structure elements from the PDB entry are shown for the native structure (at the left). The definition of secondary structure elements, shown for the structures along the unfolding simulations, is based on repeating dihedral angles (*34*). This figure was drawn with Molscript (*55*) and Raster3D (*56*).

before and after that (Figure 6). From 600 to 1020 ps, there is a progressive loss of native and non-native interactions, shown by the N-terminus with segments distant in sequence (Figure 6B−D). A detailed analysis was carried out to characterize the most persistent interactions of both termini during the N-terminal opening (880−1020 ps). Residues 1−13 make hydrogen bonds only among themselves and a few van der Waals interactions with the hinge loop. This loop displays hydrogen bonding interactions with itself, and hydrophobic contacts with residues belonging to α2 helix, mostly between Ser16-Thr17 and Gln28-Ser32-Arg33. On the other hand, residues 116−124 are connected to the rest of the molecule by several interactions. Besides the charged conserved interactions, Asp121−Lys66, Val124 COO^-−Arg85, and Val124 COO^-−Lys104, there are van der Waals contacts lasting from 30 to 70% of the time span and connecting residues Val116, Phe120, Ala122, and Ser123 with residues Leu51, Cys65, Lys66, Lys104, Ile106, and Leu107. The interactions between the C-terminus and the residues on the opposite segment of residues 104−107 anchor the C-terminus to residues 101−111 which display both persistent hydrogen-bonded and nonpolar interactions with residues 80−82 and 71−75. After the transient opening seen in Figure 6D, the N-terminus establishes non-native interactions with distant segments (Figure 6E,F) and again fluctuates closer to the body.

Although the opening of the N-terminus occurs late (880−1020 ps) in the unfolding pathway, the protein still retains residual secondary structure: the α-helical and *β*-strand content are 9 ± 3 and 13 ± 4%, respectively, based on repeating dihedral angles (*34*). For comparison, the crystal structure contains 21 and 41% α and *β* structure, respectively. In particular, in this time window, the most persistent native secondary structural elements with their relative stability are as follows: helices α2 > α1 and strands *β*3−*β*6 > *β*2−*β*3 > *β*4−*β*5 (Figure 6).

N498_MD4. The sequence of events during the MD4 simulation is grossly similar to that observed in MD1. There is an initial loosening of the hydrophobic core due to the N-terminal helix and the C-terminal hairpin undergoing a separating motion. Then α1 moves toward the V2 lobe of the molecule where it displays interactions with residues 46−51 and α2. The hinge loop (residues 15−22) is outside, exposed to the solvent since the early steps of the unfolding simulation. Subsequently, the N-terminal segment again moves closer to the rest of the structure, making contacts with residues of the C-terminal hinge loop. A significant displacement of the N-terminus and the hinge loop occurs around 2.8 ns. These segments are completely exposed to the solvent up to ∼3.9 ns (Figure 5B). The N-terminus undergoes subsequent expansions and contractions away from and against the rest of the molecule, resulting in a

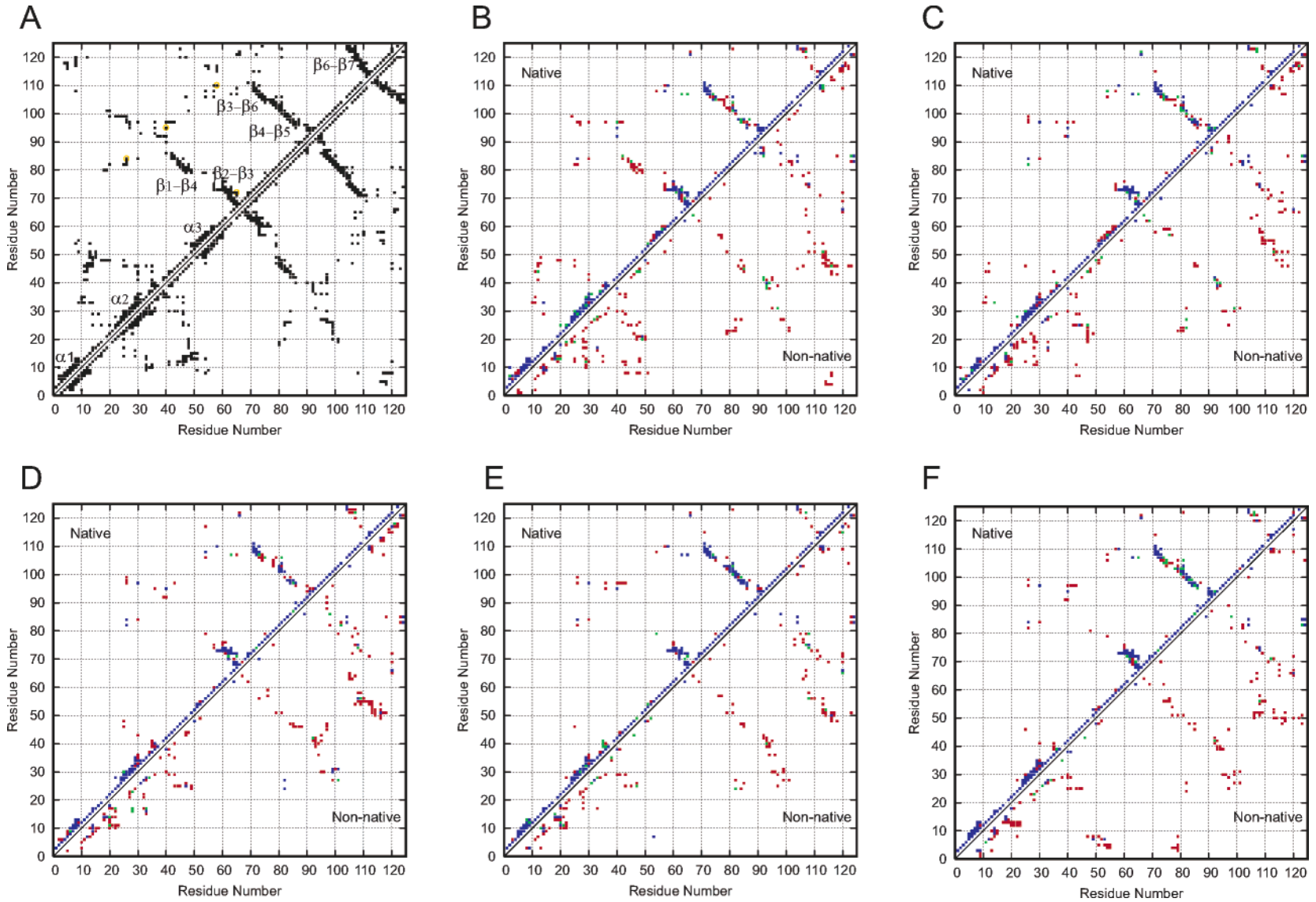

FIGURE 6: N498_MD1 heavy atom contact maps: (A) the crystal structure, (B) 600−740 ps, (C) 740−880 ps, (D) 880−1020 ps, (E) 1020−1160 ps, and (F) 1160−1300 ps. Contacts are defined as having heavy atom distances between non-neighboring residues of ≤4.6 Å except for aliphatic carbon atoms, where a distance of ≤5.6 Å is used. Native contacts and non-native contacts are shown above and below the diagonal, respectively. The contacts are colored: blue, intact 80−100% of the time period; green, intact 60−80% of the time; and red, intact 10−60% of the time. In panel A, the secondary structure elements are labeled and the disulfide bonds are denoted with a yellow circle.

change of the helix position. During the fluctuation into the solvent, the helix unfolds and refolds and the conformation of the whole segment of residues 1−22 is equally highly dynamic. Within the specific time window of 3380−3660 ps, the N-terminus has no contact interface with the rest of the molecule and adopts an orientation similar to that found in the N-terminally swapped dimer (Figure 5B). Although this conformation is sampled in the part of the trajectory when the protein has been thought to enter the denatured state, the overall shape of the protein is retained and residual helical structure (∼10 ± 3%) is still present. This large movement of the N-terminus, reflected in an increase in the C_α rmsd (Figure 2), is not observed in other simulations. On the other hand, the C-terminal segment, though partially exposed to the solvent, is still linked to other segments of the structure. Ionic interactions (Lys104, Lys98, Asp121, and Val124 COO^-) as well as hydrophobic contacts, mostly involving Val116, Pro117, and Val118, tighten the C-terminus to the protein body.

It is interesting to note that the segment comprised of residues 15−22 adopts transient α-helical structure later during the unfolding (∼5.5−6.5 ns). In the same time window, the N-terminus undergoes another large movement away from the core, as reflected in a second maximum in the C_α rmsd plot (Figure 2). An α-helical conformation for residues 16−22 was found in one of the two chains of the N-dimer structure (Figure 1B).

N498_MD2 and N498_MD3. Early in the MD3 simulation (∼240 ps), the hinge loop (residues 15−22) becomes fully exposed to the solvent. On the contrary, the α1 helix, although displaced from its native position, is never completely detached from the rest of the molecule because of its persistent N-terminal end interactions. Along the whole trajectory, the C-terminal segment displays charged interactions (Lys104−Val124 COO^-, Lys66−Val124 COO^-, and Asp121−Lys66), as well as numerous hydrophobic contacts. Similar restraints to the C-terminus mobility are found in the MD2 simulation (Lys104−Val124 COO^-, Lys104−Asp121, Arg85−Val124 COO^-, and Asp121−Lys66) compared to MD3. On the other hand, by 600 ps the hinge loop becomes exposed to solvent. In the 825−1020 ps time interval, the N-terminus pulls away from the core but retains a few contacts, mainly involving the Met13 side chain. Apart from this partial opening, the N-terminus fluctuates close to the protein.

The formation of charged interactions by the C-terminus is an early and recurrent event in the unfolding pathways of MD1−MD4. In the native structure, positively charged residues such as Lys66 and Lys104 are located on the same side of the molecule (V1 lobe), spatially close to the negative charges of Asp121 and Val124 COO^- (N_ζ66−$O_{\delta 2}$121, 5.6 Å; O124−N_ζ104, 6.5 Å). Two other basic residues, Lys98 and Arg85, lie on the opposite side, in the V2 lobe, quite distant from the charged residues at the C-terminus (O124−$N_{\eta 2}$85, 12.3 Å; O124−N_ζ98, 17.8 Å; $O_{\delta 1}$121−$N_{\eta 1}$85, 13.1 Å). However, the distance between β7 and the V2 lobe is decreased during unfolding, when the V-shaped motif opens and the C-terminal segment (residues 116−124) moves a little farther from its paired β6 strand. In each of the neutral−pH unfolding simulations, the most persistent and the earliest-formed electrostatic interaction is that involving Val124 COO^- and Lys104 at the end of the opposite strand.

Since it was reported that at high temperatures the effect of charge−charge interactions may be overestimated (*35*), we tested the occurrence of charged clusters at C-terminal side by performing an unfolding simulation at 373 K (data not shown). Even at this temperature, the C-terminus forms electrostatic interactions in very early stages of the pathway, as in the 498 K simulations.

Low pH. To reproduce the harsh unfolding conditions used in the acid lyophilization experiments, simulations were performed at the same temperature but using a low pH. Unfolding occurs much more rapidly at low pH, leading to a more expanded denatured state than at neutral pH, as also reflected in a larger gyration radius (18.0 ± 0.6 Å vs 16.0 ± 0.2 Å, each value calculated by averaging over the four simulations in the 4−10 ns interval).

The dynamic behavior of the termini shows large heterogeneity across the four simulations. In all of the simulations, there is an opening of both the N-terminus and the C-terminus when denatured structures are sampled along the unfolding trajectory. However, a comparative analysis reveals no chronological order for the dislocation of the termini from the body of the molecule.

In the early unfolding steps of L498_MD1, neither terminus comes apart, and both continue to keep interactions with the rest of the chain which rapidly loses secondary and tertiary structure. The two termini interact with each other up to 2.6 ns when they separate and fluctuate on opposite sides of the molecule. At 3.2−4.9 ns, the C-terminus is fully exposed to the solvent (Figure 5C) whereas the N-terminus, although exposed, retains a contact interface with the body. Subsequently, conformations having both termini opened are sampled (Figure 5C).

In L498_MD2, the complete exposure to solvent of the N-terminus (∼1 ns) precedes that of the C-terminus (∼1.8−2 ns). On the other hand, early in the L498_MD3 simulation (∼200 ps), the terminal arms simultaneously swing out and interact with each other on the same side of the molecule (Figure 5D). A full opening occurs later for both termini (after 4.5 ns) (Figure 5D). Finally, the N-terminus pulls away from the core early in the L498_MD4 trajectory, and at ∼1 ns, it is fully exposed to the solvent. Over the next 1.5 ns, the C-terminus becomes exposed as well.

Collectively, the unfolding simulations at low pH show that the C-terminus is significantly more mobile than at neutral pH. Yet a complete separation occurs only when the protein has already entered the denatured state (Figure 5C,D). The protonation of both the Asp121 side chain and the Val124 carboxylate group may favor the opening of the C-terminus, as ionic interactions that anchor residues 116−124 to the body of the molecule are prevented. The dynamic behavior of the termini at neutral and low pH can be estimated by monitoring C_α−C_α distances between residues of the terminal arms and residues located close to the center of the molecule (those showing the lowest rms fluctuation in N298_MD and L298_MD) (Figure 7). Over the course of the simulations, the C-terminus shows larger displacements at low pH than at neutral pH, while the N-terminus has a high mobility under both pH conditions (Figure 7).

DISCUSSION

RNase A is a versatile monomeric protein that can aggregate via different modes of three-dimensional (3D)

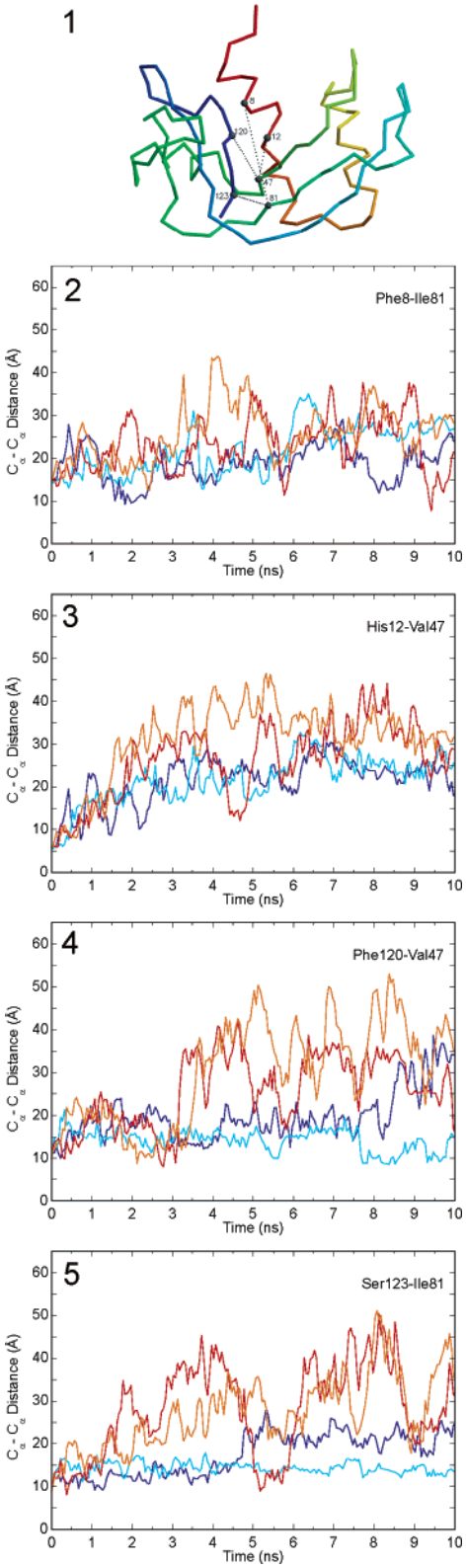

FIGURE 7: Representative $C_\alpha-C_\alpha$ distances between residues located close to the center of the molecule (Val47 and Ile81) and residues belonging to the N-terminus (Phe8 and His12) and the C-terminus (Phe120 and Ser123), calculated for two unfolding simulations at each pH: (1) localization of the distance pairs in the structure, (2) Phe8 $C_\alpha-$Ile81 C_α, (3) His12 $C_\alpha-$Val47 C_α, (4) Phe120 $C_\alpha-$Val47 C_α, and (5) Ser123 $C_\alpha-$Ile81 C_α. The distances are depicted in cyan (N498_MD1), blue (N498_MD4), red (L498_MD1), and orange (L498_MD4). The distance values are obtained by averaging over structures each 50 ps. Panel 1 of this figure was drawn with Molscript (*55*) and Raster3D (*56*).

domain swapping to form dimers and higher-order aggregates under destabilizing conditions. In particular, upon lyophilization in a 40−50% acetic acid solution, the protein forms two types of metastable dimers with different quaternary structures (*9*, *10*, *15*, *16*). Under these conditions, the yield of dimers is ∼20% with the most abundant dimer formed by domain swapping of the C-terminal segment (C-dimer). In the second domain-swapped dimer structure, it is the N-terminal α-helix of one subunit to be folded onto the body of the other and vice versa (N-dimer). The ratio of C- to N-dimer amounts is ∼4:1. The 3D structural characterization of the dimers has shown that the N-dimer has a more compact interface formed by a β-strand pairing, which leads to the formation of a six-stranded β-sheet across the interface. On the other hand, the C-dimer exhibits a structurally looser assembly with only a few additional hydrogen bonds. The two dimers also show different dynamic properties with the C-dimer undergoing larger conformational changes in its quaternary structure by MD (L. Vitagliano, personal communication).

Recent investigations show that the swapped dimers can also be obtained avoiding the lyophilization step, by using high protein concentrations, high temperatures, and destabilizing solvents (*23*). The prevalence of the C-dimer versus the N-dimer can be reversed depending on strong versus mild unfolding conditions. Some indirect evidence also indicates that RNase A forms traces of dimers under conditions similar to physiological ones (*36*).

MD unfolding simulations of the RNase A monomer were carried out to gain insight into the pathway leading to domain-swapped dimers. Simulations at room temperature were also performed as a control and showed that there is an opening of the two arms of the V-shaped motif. This is in line with the breathing motion of the β-sheets, previously detected by essential dynamics and crystallographic studies, and proposed to play a functional role (*33*, *37*, *38*). In N298, the distance between Thr45 and Phe120, which reflects the breathing motion, is in close agreement with that obtained from a previous MD simulation study and from a survey of X-ray structures of RNase A (*37*). As far as the behavior of the terminal segments is concerned, dynamics at 298 K show that most of the hydrogen bonds anchoring these segments are well preserved. In particular, the interaction between His12 and Thr45, which are very rigid residues of the active site, is very stable, in agreement with experimental data (*27*, *39*), as well as previous MD simulations of RNase A (*37*). In addition, the hydrogen bonds pairing β7 and β6 are very stable during the simulations, in line with the significant protection against H−D exchange in this region (*40*).

In the MD simulations of thermal denaturation, the temperature is increased to 498 K. The early steps of unfolding are characterized by a separating motion of the N-terminal helix and the C-terminal β-hairpin, leading to a loosening of the main hydrophobic core. This is consistent with experimental data indicating that, before the cooperative main unfolding transition, local changes proceed via the relaxation of tertiary interactions between the C-terminal β-hairpin and the N-terminal helix (*41*). The analysis of subsequent events was focused on the significant displacements of the terminal segments from the core of the molecule. In any case, our unfolding simulations indicate a remarkable stability of the α-helices. Experimentally, the

three helices in RNase A are marginally stable as short fragments in solution at room temperature in the absence of tertiary interactions (*42*). In addition, a number of circular dichroism (CD), FT-IR, and SAXS/FT-IR studies suggest that nonrandom structures still exist in the thermally denatured state of RNase A (*41*, *43*−*46*). Most of these studies indicate that the α-helical content decreases to only half that of the native state. In contrast, stable hydrogen-bonded structure could not be detected by a FT-IR study (*47*) or NMR NH exchange experiments (*48*).

The main result of our MD study is the finding of a transient opening of the N-terminal arm during two out of four independent unfolding trajectories at neutral pH. In one simulation, the N-terminal segment loses its contacts with the main body of the molecule. This full exposure to solvent lasts for ∼140 ps and occurs after ∼900 ps of simulation; at this point, the molecule contains significant α-helical content and some residual extended structure. In the other simulation, the N-terminus undergoes a more pronounced and long-lasting (∼240 ps) outward movement, leading to an overall chain conformation similar to that found in the N-dimer. This dislocation of the N-terminal segment occurs late along the unfolding trajectory (∼3.6 ns) when the molecule has already lost its *β*-structure but still retains some α-helical structure. The overall backbone shape is also preserved, perhaps restrained by the presence of four disulfide bridges. No significant opening of the C-terminal arm is observed in any of the simulations at neutral pH. The mobility of the C-terminal region appears to be restricted by the disulfide bridge between residues 58 and 110 which anchors the end of the *β*6 strand to the body of the molecule, as well as by charged interactions involving residue Asp121 and the C-terminal carboxylate group on Val124 on strand *β*7. In particular, the recurrent formation of the ionic interaction between the Val124 and Lys104, which are only 6.5 Å apart in the native structure, points to a possible role played by this residue in decreasing the mobility of the C-terminus.

It is worth noting that a critical factor in obtaining detectable amounts of dimers is the high concentration of the protein or the lyophilization procedure, which removes most of the solvation shell separating individual molecules in solution, thus indirectly increasing the concentration. Yet this factor has to be coupled with destabilizing conditions (solvent and/or high temperature) to induce dimerization. Therefore, in highly concentrated solutions, direct interactions of protein molecules could ease the opening of partially dislocated N-terminal arms by providing further contact surfaces.

Furthermore, even at very high protein concentrations, the percentage of macromolecules that experimentally form swapped dimers is rather low (total dimer aggregates are less than 20%; the N-terminal dimer is always less than 10%). This seems to indicate that the detachment of terminal arms is the limiting event in the swapped dimer formation. In this context, it is not surprising that the conformational sampling given by the four 10 ns unfolding simulations does not result in selective displacement of the N-terminus for all simulations.

The termini behave differently in MD simulations at very low pH and high temperature, which aim to mimic the strong unfolding conditions of the dimerization from lyophilization in an acetic acid solution. In fact, the C-terminus detaches from the body of the molecule, to become fully exposed to the solvent. This opening is favored by the protonation of the two negatively charged groups of Asp121 and the Val124 terminal carboxylate. An opening of the N-terminal segment is also observed; however, our results indicate that a complete dislocation of the C-terminus occurs from a substantially unfolded state.

It is possible that RNase A must unfold completely for the transformation to the domain-swapped C-dimer, whereas the association of monomers into the domain-swapped N-dimer may occur when the protein is only partially unfolded. This idea is in line with biochemical experiments that indicate that the yield of the N-dimer varies little going from mild to strong unfolding conditions (from 2.2 to 8.7%), whereas the percentage of C-dimer increases appreciably (from 0.8 to 18%) (*23*). At neutral pH, the prevalence of the N-dimer can be ascribed to the higher mobility of the N-terminal arm, which results in a large population of partially unfolded monomers with exposure of the N-terminus. On the other hand, at very low pH, MD simulations indicate that both terminal arms exhibit high mobility.

In conclusion, the picture emerging from our MD unfolding studies is that the same protein can have different pathways for 3D domain swapping. The C-terminal swapping requires a substantial unfolding of the monomers, similar to what has been suggested for proteins such as p13suc1 (*25*, *49*) and protein L (*50*). On the other hand, the N-terminal swapping can occur through partial unfolding of the monomers, as seems to be the case for the diphtheria toxin (*1*) and bovine seminal ribonuclease (BS-RNase) (*55*). BS-RNase is the only naturally dimeric enzyme from the "pancreatic-type" superfamily (*52*). It is a homodimer, maintained by two intersubunit disulfide bonds and various noncovalent interactions. Interestingly, this enzyme, the sequence of which is 80% identical with that of RNase A, exists in vivo as two dimeric forms in equilibrium: a swapped dimer (MXM) with the two subunits exchanging their N-terminal helix (*53*, *54*) and an unswapped dimer (M = M), with each protomer folding onto itself. Although the MXM quaternary structure is completely different from that of the RNase A N-dimer, the occurrence of the N-terminal swapping under physiological conditions supports the easier opening of this terminal segment in RNases, in agreement with our MD results. A further observation in line with these findings is the occurrence of a different N-terminal domain-swapped RNase structure, which was artificially obtained by engineering human ribonuclease (*7*). On the basis of our MD simulations and the results discussed above, we propose that only N-terminal domain swapping is present in the traces of the RNase A swapped dimer suggested to exist in vivo (*36*). However, the detailed quaternary structure of this dimer remains to be elucidated.

ACKNOWLEDGMENT

L.E. gratefully acknowledge Dr. Luigi Vitagliano for insightful discussions and Dr. Darwin O. V. Alonso for help with the computational work.

REFERENCES

1. Bennett, M. J., Schlunegger, M. P., and Eisenberg, D. (1995) 3D Domain swapping: a mechanism for oligomer assembly, *Protein Sci. 4*, 2455−2468.

2. Schlunegger, M. P., Bennett, M. J., and Eisenberg, D. (1997) Oligomer formation by 3D domain swapping: A model for protein assembly and misassembly, *Adv. Protein Chem. 50*, 61−122.
3. Bennett, M. J., Choe, S., and Eisenberg, D. (1994) Refined structure of dimeric diphtheria toxin at 2.0 Å resolution, *Protein Sci. 3*, 1444−1463.
4. Liu, Y., and Eisenberg, D. (2002) 3D domain swapping: as domains continue to swap, *Protein Sci. 11*, 1285−1299.
5. Newcomer, M. E. (2002) Protein folding and three-dimensional domain swapping: A strained relationship? *Curr. Opin. Struct. Biol. 12*, 48−53.
6. Rousseau, F., Schymkowitz, J. W. H., and Itzhaki, L. S. (2003) The unfolding story of three-dimensional domain swapping, *Structure 11*, 243−251.
7. Canals, A., Pous, J., Guasch, A., Benito, A., Ribo, M., Vilanova, M., and Coll, M. (2001) The structure of an engineered domain-swapped ribonuclease dimer and its implications for the evolution of proteins toward oligomerization, *Structure 9*, 967−976.
8. Cohen, F. E., and Prusiner, S. B. (1998) Pathologic conformations of prion proteins, *Annu. Rev. Biochem. 67*, 793−819.
9. Liu, Y., Hart, P. J., Schlunegger, M. P., and Eisenberg, D. (1998) The crystal structure of a 3D domain-swapped dimer of RNase A at a 2.1-Å resolution, *Proc. Natl. Acad. Sci. U.S.A. 95*, 3437−3442.
10. Liu, Y., Gotte, G., Libonati, M., and Eisenberg, D. (2001) A domain-swapped RNase A dimer with implications for amyloid formation, *Nat. Struct. Biol. 8*, 211−214.
11. Sinha, N., Tsai, C. J., and Nussinov, R. (2001) A proposed structural model for amyloid fibril elongation: Domain swapping forms an interdigitating β-structure polymer, *Protein Eng. 14*, 93−103.
12. Janowski, R., Kozak, M., Jankowska, E., Grzonka, Z., Grubb, A., Abrahamson, M., and Jaskolski, M. (2001) Human cystatin C, an amyloidogenic protein, dimerizes through three-dimensional domain swapping, *Nat. Struct. Biol. 8*, 316−320.
13. Piccoli, R., Di Donato, A., and D'Alessio, G. (1988) Co-operativity in seminal ribonuclease function. Kinetic studies, *Biochem. J. 253*, 329−336.
14. Vitagliano, L., Adinolfi, S., Sica, F., Merlino, A., Zagari, A., and Mazzarella, L. (1999) A potential allosteric subsite generated by domain swapping in bovine seminal ribonuclease, *J. Mol. Biol. 293*, 569−577.
15. Crestfield, A. M., Stein, W. H., and Moore, S. (1962) On the aggregation of bovine pancreatic ribonuclease, *Arch. Biochem. Biophys. 1*, 217−222.
16. Gotte, G., and Libonati, M. (1998) Two different forms of aggregated dimers of ribonuclease A, *Biochim. Biophys. Acta 1386*, 106−112.
17. Sorrentino, S., Barone, R., Bucci, E., Gotte, G., Russo, N., Libonati, M., and D'Alessio, G. (2000) The two dimeric forms of RNase A, *FEBS Lett. 466*, 35−39.
18. Gotte, G., Bertoldi, M., and Libonati, M. (1999) Structural versatility of bovine ribonuclease A. Distinct conformers of trimeric and tetrameric aggregates of the enzyme, *Eur. J. Biochem. 265*, 680−687.
19. Nenci, A., Gotte, G., Bertoldi, M., and Libonati, M. (2001) Structural properties of trimers and tetramers of ribonuclease A, *Protein Sci. 10*, 2017−2027.
20. Liu, Y., Gotte, G., Libonati, M., and Eisenberg, D. (2002) Structures of the two 3D domain-swapped RNase A trimers, *Protein Sci. 11*, 371−380.
21. Matousek, J., Gotte, G., Pouckova, P., Soucek, J., Slavik, T., Vottariello, F., and Libonati, M. (2003) Antitumor activity and other biological actions of oligomers of ribonuclease A, *J. Biol. Chem. 278*, 23817−23822.
22. Merlino, A., Vitagliano, L., Ceruso, M. A., and Mazzarella, L. (2004) Dynamic properties of the N-terminal swapped dimer of ribonuclease A, *Biophys. J. 86*, 2382−2391.
23. Gotte, G., Vottariello, F., and Libonati, M. (2003) Thermal aggregation of ribonuclease A. A contribution to the understanding of the role of 3D domain swapping in protein aggregation, *J. Biol. Chem. 278*, 10763−10769.
24. Daggett, V. (2002) Molecular dynamics simulations of the protein unfolding/folding reaction, *Acc. Chem. Res. 35*, 422−429.
25. Alonso, D. O. V., Alm, E., and Daggett, V. (2000) Characterization of the unfolding pathway of the cell-cycle protein p13suc1 by molecular dynamics simulations: implications for domain swapping, *Structure 8*, 101−110.
26. Berisio, R., Sica, F., Lamzin, V. S., Wilson, K. S., Zagari, A., and Mazzarella, L. (2002) Atomic resolution structures of ribonuclease A at six pH values, *Acta Crystallogr. D58*, 441−450.
27. Esposito, L., Vitagliano, L., Sica, F., Sorrentino, G., Zagari, A., and Mazzarella, L. (2000) The ultrahigh-resolution crystal structure of ribonuclease A containing an isoaspartyl residue: Hydration and sterochemical analysis, *J. Mol. Biol. 297*, 713−732.
28. Levitt, M. (1990) *ENCAD, Computer Program, Energy Calculations and Dynamics*, Molecular Applications Group, Palo Alto, CA.
29. Levitt, M., Hirshberg, M., Sharon, R., and Daggett, V. (1995) Potential energy function and parameters for simulations of the molecular dynamics of proteins and nucleic acids in solutions, *Comput. Phys. Commun. 91*, 215−231.
30. Levitt, M., Hirshberg, M., Sharon, R., Laidig, K. E., and Daggett, V. (1997) Calibration and testing of a water model for simulation of the molecular dynamics of proteins and nucleic acids in solution, *J. Phys. Chem. B 101*, 5051−5061.
31. Kell, G. S. (1967) Precise representation of volume properties of water at one atmosphere, *J. Chem. Eng. Data 12*, 66−68.
32. Beck, D. A. C., Armen, R. S., and Daggett, V. (2005) Cutoff size need not strongly influence molecular dynamics results for solvated polypeptides, *Biochemistry 44*, 609−616.
33. Vitagliano, L., Merlino, A., Zagari, A., and Mazzarella, L. (2002) Reversibile substrate-induced domain motions in ribonuclease A, *Proteins 46*, 97−104.
34. Daggett, V., Kollman, P. A., and Kuntz, I. D. (1991) A molecular dynamics simulation of polyalanine: An analysis of equilibrium motions and helix-coil transitions, *Biopolymers 31*, 1115−1134.
35. Thomas, A. S., and Elcock, A. H. (2004) Molecular simulations suggest protein salt bridges are uniquely suited to life at high temperatures, *J. Am. Chem. Soc. 126*, 2208−2214.
36. Park, C., and Raines, R. T. (2000) Dimer formation by a monomeric protein, *Protein Sci. 9*, 2026−2033.
37. Merlino, A., Vitagliano, L., Ceruso, M. A., Di Nola, A., and Mazzarella L. (2002) Global and local motions in ribonuclease A: A molecular dynamics study, *Biopolymers 65*, 274−283.
38. Merlino, A., Vitagliano, L., Ceruso, M. A., and Mazzarella, L. (2003) Subtle functional collective motions in pancreatic-like ribonucleases: From ribonuclease A to angiogenin, *Proteins 53*, 101−110.
39. Wlodawer, A. (1985) Structure of bovine pancreatic ribonuclease by X-ray and neutron diffraction, in *Biological macromolecules and assembly* (Jurnak, F., and McPherson, A., Eds.) pp 394−439, Wiley, New York.
40. Neira, J. L., Sevilla, P., Menendez, M., Bruix, M., and Rico, M. (1999) Hydrogen exchange in ribonuclease A and ribonuclease S: evidence for residual structure in the unfolded state under native conditions, *J. Mol. Biol. 285*, 627−643.
41. Navon, A., Ittah, V., Laity, J. H., Scheraga, H. A., Haas, E., and Gussakovsky, E. E. (2001) Local and long-range interactions in the thermal unfolding transition of bovine pancreatic ribonuclease A, *Biochemistry 40*, 93−104.
42. Neira, J. L., and Rico, M. (1997) Folding studies on ribonuclease A, a model protein, *Folding Des. 2*, R1−R11.
43. Labhardt, A. M. (1982) Secondary structure in ribonuclease. I. Equilibrium folding transitions seen by amide CD, *J. Mol. Biol. 157*, 331−355.
44. Seshadri, S., Oberg, K. A., and Fink, A. L. (1994) Thermally denatured ribonuclease A retains secondary structure as shown by FTIR, *Biochemistry 33*, 1351−1355.
45. Torrent, J., Connelly, J. P., Coll, M. G., Ribó, M., Lange, R., and Vilanova, M. (1999) Pressure versus heat-induced unfolding of ribonuclease A: The case of hydrophobic interactions within a chain-folding initiation site, *Biochemistry 38*, 15952−15961.
46. Sosnick, T. R., and Trewhella, J. (1992) Denatured states of ribonuclease A have compact dimensions and residual secondary structure, *Biochemistry 31*, 8329−8355.
47. Fabian, H., and Mantsch, H. H. (1995) Ribonuclease A revisited: Infrared spectroscopic evidence for lack of native-like secondary structure in the thermally denatured state, *Biochemistry 34*, 13651−13655.
48. Robertson, A. D., and Baldwin, R. L. (1991) Hydrogen exchange in thermally denatured ribonuclease A, *Biochemistry 32*, 5222−5232.
49. Rousseau, F., Schymkowitz, J. W., Wilkinson, H. R., and Itzhaki, L. S. (2001) Three-dimensional domain swapping in p13suc1

occurs in the unfolded state and is controlled by conserved proline residues, *Proc. Natl. Acad. Sci. U.S.A. 98*, 5596−5601.
50. Kulman, B., O'Neill, J. W., Kim, D. E., Zhang, K. Y., and Baker, D. (2001) Conversion of monomeric protein L to an obligate dimer by computational protein design, *Proc. Natl. Acad. Sci. U.S.A. 98*, 10687−10691.
51. Piccoli, R., De Lorenzo, C., Dal Piaz, F., Pucci, P., and D'Alessio, G. (2000) Trypsin shed light on the singular case of seminal RNase a dimer with two quaternary conformations, *J. Biol. Chem. 11*, 8000−8006.
52. D'Alessio, G., Di Donato, A., Mazzarella, L., and Piccoli, R. (1997) Seminal ribonuclease: the importance of diversity, in *Ribonucleases: Structures and Functions* (D'Alessio, G., and Riordan, J. F., Eds.) pp 383−423, Academic Press, New York.
53. Piccoli, R., Tamburrini, M., Piccialli, G., Di Donato, A., Parente, A., and D'Alessio, G. (1992) The dual-mode quaternary structure of seminal RNase, *Proc. Natl. Acad. Sci. U.S.A. 89*, 1870−1874.
54. Mazzarella, L., Capasso, S., Demasi, D., Di Lorenzo, G., Mattia, C. A., and Zagari, A. (1993) Bovine seminal ribonuclease: Structure at 1.9 Å resolution, *Acta Crystallogr. D49*, 389−402.
55. Kraulis, P. J. (1991) MOLSCRIPT: A program to produce both detailed and schematic plots of protein structures, *J. Appl. Crystallogr. 24*, 946−950.
56. Merritt, E. A., and Bacon, D. J. (1997) Raster3D: Photorealistic molecular graphics, *Methods Enzymol. 277*, 505−524.

BI0488350